Kink modes and surface currents associated with vertical displacement events

Janardhan Manickam,[a] Allen Boozer,[b] and Stefan Gerhardt
Princeton Plasma Physics Laboratory, Princeton University, Princeton, New Jersey 08540, USA

(Received 30 January 2012; accepted 13 July 2012; published online 2 August 2012)

The fast termination phase of a vertical displacement event (VDE) in a tokamak is modeled as a sequence of shrinking equilibria, where the core current profile remains constant so that the safety-factor at the axis, q_{axis}, remains fixed and the q_{edge} systematically decreases. At some point, the $n = 1$ kink mode is destabilized. Kink modes distort the magnetic field lines outside the plasma, and surface currents are required to nullify the normal component of the B-field at the plasma boundary and maintain equilibrium at finite pressure. If the plasma touches a conductor, the current can be transferred to the conductor, and may be measurable by the halo current monitors. This report describes a practical method to model the plasma as it evolves during a VDE, and determine the surface currents, needed to maintain equilibrium. The main results are that the onset conditions for the disruption are that the growth-rate of the $n = 1$ kink exceeds half the Alfven time and the associated surface current needed to maintain equilibrium exceeds one half of the core plasma current. This occurs when q_{edge} drops below a low integer, usually 2. Application to NSTX provides favorable comparison with non-axisymmetric halo-current measurements. The model is also applied to ITER and shows that the 2/1 mode is projected to be the most likely cause of the final disruption. © *2012 American Institute of Physics*. [http://dx.doi.org/10.1063/1.4740507]

I. INTRODUCTION

Tokamak plasmas are inherently susceptible to an axisymmetric vertical instability, particularly when they are elongated. Consequently, normal plasma operation requires feedback control of the vertical position to counter the growth of small displacements. However, circumstances such as improper or inadequate feedback control may lead to vertical displacement events (VDEs), which often culminate in disruptions. The disruption occurs on a fast time scale and carries the potential of inducing large forces on the surrounding structures, within the vessel. Understanding the unstable mode-structure and related surface currents could help ameliorate the consequences of this dangerous event. This report addresses the ideal MHD stability of the $n = 1$ kink mode starting from the initial uncontrolled vertical displacement, up to the beginning of the current quench phase, here n is the toroidal mode number.

VDEs start with a vertical displacement, which may be upward or downward, but always pushing the plasma towards some material surface. Once contact is established, the plasma starts to shrink. This process continues until the onset of a fast growing instability leads to a current quench and termination of the discharge. The instability corresponds to an $n = 1$ kink mode, see Ref. 1. The vertical motion is related to the axisymmetric, $n = 0$ instability.

The VDE evolves on a time-scale, significantly, slower than the fast, Alfvenic time-scale of the ideal kink instability. This implies that during most of the VDE, the shrinking plasma is in equilibrium and should be kink stable, until the time of the disruption. Shortly before the disruption, currents are observed in the halo current monitors. These have been determined to have an axisymmetric, $n = 0$, as well as an $n = 1$, non-axisymmetric component. The latter may be related to the observed strong non-symmetric forces acting on the nearby conducting structures and vacuum vessel. This report addresses the ideal MHD stability of the plasma during the VDE, focusing on the $n = 1$ mode, its growth-rate and associated surface currents.

A theoretical model has emerged connecting the equilibrium of a kink-deformed plasma, with currents on the plasma surface.[2–4] These currents flow parallel to the field, and counter to the core plasma current. The plasma deformation is driven by a kink instability, and estimates of these currents can be obtained by determining the δ-function surface current required to ensure $\mathbf{B} \cdot \mathbf{n} = \mathbf{0}$, on the plasma-vacuum interface. The growth of an n = 1 kink twists the open magnetic field lines just outside the plasma, which induces a voltage proportional to the growth rate between one intersection of these magnetic field lines with the wall to the other. When this voltage becomes sufficiently great, a current is driven, which provides force balance and makes the growth rate of the kink and this halo current proportional to the resistivity experienced by this current. In most cases, a strong halo current arises when q_{edge} is slightly less than two. To precisely calculate this effect, a code that can find helical equilibria with a strong halo current would be required. Such a code does not exist so a simpler procedure is adopted. The plasma boundary is treated as a resistive wall and the surface current that would be required to maintain force balance in the presence of the kink is calculated.

This report extends previous theoretical analyses, which was confined to cylindrical, Shafranov, plasma models, to

[a]manickam@pppl.gov.
[b]Also at the Department of Applied Physics and Applied Mathematics, Columbia University, New York, New York 10027, USA.

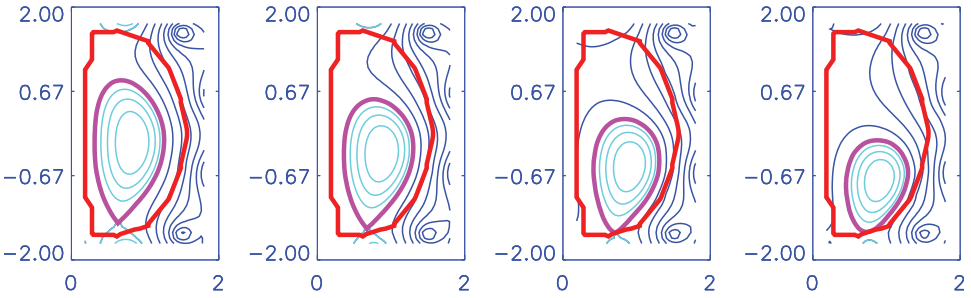

FIG. 1. Equilibrium sequence of a VDE in an NSTX discharge, shot No. 139540, at 3 ms. Intervals starting at $t = 0.322$ s into the discharge. The discharge terminated at about $t = 0.338$ s. The last usable equilibrium was at $t = 0.331$ s. This was used to simulate the disruption phase. The last closed flux surface is highlighted in magenta.

numerical modeling of realistic plasmas based on experimental observations. A detailed study is presented of two NSTX discharges, using the best estimates of plasma profiles from experimental observations and modeling. This is followed by an application to ITER, using an equilibrium based on transport simulation. Results in JET geometry are also presented. The main results describe the onset conditions for the disruption and estimates of the surface current.

A comprehensive model requires the use of non-linear time-dependent MHD codes, coupled to a transport code treating the plasma, halo and material surfaces self-consistently. Research along these lines is still evolving and has provided insight on this complex problem, particularly relating the instability to the forces within the machine.[5]

This study is based on a simple linear ideal MHD model. However, it provides meaningful information on stability boundaries, mode structures, and growth-rates. In particular, since the growth-rate is a measure of the energy released by the instability, it provides a window on the forces involved.

The following sections describe: the plasma model, a method to determine the surface currents; application to NSTX; the results for ITER and JET geometries; and conclusions.

II. PLASMA MODEL

The evolution of the VDE is described by a sequence of plasma equilibria, with shrinking boundaries as the outer flux surfaces are lost, the safety-factor at the plasma boundary reduces continuously. These features are shown in Figures 1 and 2. The equilibria were reconstructed using LRDFIT,[6] for NSTX shot number 139540 at 3 ms intervals, starting at $t = 0.322$ s. Figure 1 shows the poloidal flux contours corresponding to the sequence of equilibria. Figure 2 shows details of the safety factor and pressure gradient profiles for the equilibria in Fig. 1. Figure 3 shows the evolution of key plasma parameters, including, z_{axis}, q_{edge}, the normalized beta, β_N, the soft-x-ray signal, the plasma current, I_p, and the measured "halo" currents. These are separated into the axisymmetric, $n = 0$ and non-axisymmetric $n = 1$ components.

The plasma starts the downward motion at about $t = 0.320$ s, outside the range of the plot. The edge safety-factor, q_{edge}, starts to drop at about 0.322 s, decreasing steadily, dropping below 2 at about $t = 0.3325$ s. The halo currents are first observed at $t = 0.331$ s, at about the same time β starts to drop. The plasma current starts to collapse a few milli-seconds later, at about $t = 0.3345$ s. Note that the entire event evolves over approximately 8 ms, a time scale which is much longer than the Alfvén time.

The sequence starts when the plasma drifts from the mid-plane starting a steady drop in q as the plasma shrinks. A few milli-seconds later there is a nearly concurrent start of the halo current, thermal quench, and onset of MHD, followed, a few milli-seconds later, by the start of the current quench phase. This sequence is also observed in the other discharge, 141641, which will be discussed later in this report. Details of the halo current measurement techniques are described in Ref. 11.

In NSTX, the correlation of the halo current with the current quench is somewhat complicated.[13] Most disruptions have a relatively shorter Halo current pulse than the current quench time; however, in pure VDEs the duration of the halo current can be longer than the current quench time and is observed before the start of the final current quench. Figures 3 and 7 show examples of these two conditions.

Ideally, for stability analysis, a sequence of plasma equilibria should be computed by fitting experimental data at time-slices close to the final disruption. This is not always possible as the experimental diagnostics may not be tuned to the shifting plasma location and key diagnostics may not be triggered in a timely manner. To overcome this, we have developed a model to mimic this sequence. We start from the closest valid equilibrium, representing a stable point, before the disruption. Starting from this equilibrium, a sequence of equilibria is generated as follows:

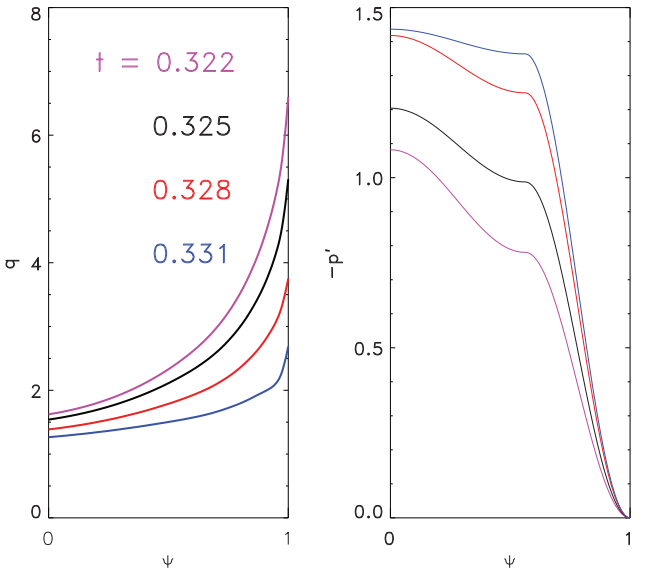

FIG. 2. The plasma profiles for the safety-factor q and negative of the pressure gradient, $\frac{-dP}{d\psi}$, for the four cases, shown in Fig. 1. Note that as the plasma shrinks, q_{edge} reduces and approaches 2.0.

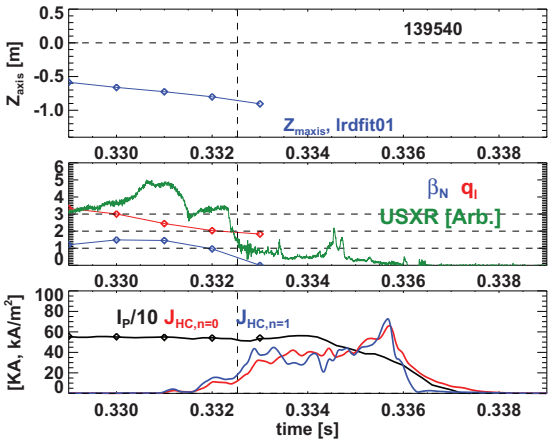

FIG. 3. Evolution of Z_{axis} (top panel), q_{edge}, and β_N (middle panel) during the last 15 ms of a VDE in NSTX, shot No. 139540. The plasma current, black, and halo current measurements for $n=0$, red; and $n=1$, blue are shown in the bottom panel. Note that q_{edge} is continuously decreasing and drops below 2 at approximately $t=0.332$ s. The halo current saturates at that time, and the disruption follows at $t=0.3345$ s.

- Select an inner flux surface from the equilibrium, obtain the **x,z** values, to be used as the plasma boundary of a new equilibrium, e.g.,

$$\Psi_b = b * (\Psi_{\text{lim}} - \Psi_{\text{axis}}),$$

  where $0.0 < b < 1.0$.
- Truncate and renormalize the equilibrium profiles $\langle \mathbf{J}\cdot\mathbf{B}\rangle/\langle B^2\rangle$ and dp/dΨ, e.g., using $\chi = \Psi/\Psi_b$, we interpolate the plasma functions as follows:

$$f(\chi)(0:1) = f(\Psi)(0:\Psi_b).$$

- Use a fixed boundary equilibrium code, JSOLVER,[7] to obtain a numerical equilibrium.

This procedure is illustrated in Figure 4. The figure on the left shows a selected flux surface of the initial stable

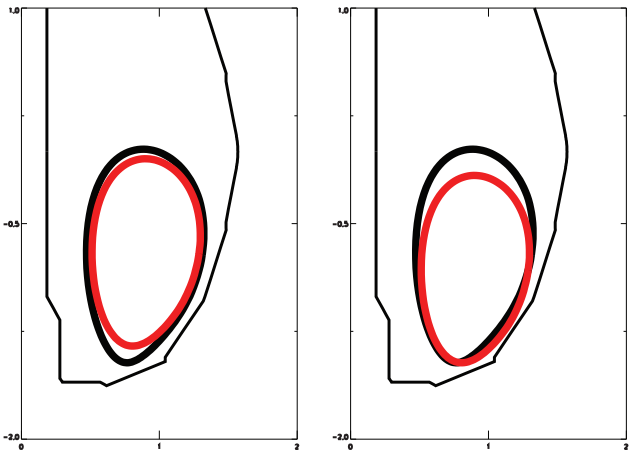

FIG. 4. Method used to extend the equilibrium sequence to simulate the disruption phase. A selected inner flux surface is shifted to represent the new bounding surface for a new fixed-boundary equilibrium calculation. The figure on the left shows the 99% flux surface in black, at $t=0.331$ and $q_{edge} \approx 2.5$, and an inner flux surface corresponding to $q_{edge} \approx 2.1$. The figure on the right shows the 2.1 surface displaced downwards to rest against the limiter (not shown). The curves overlap, on the right because the inner flux surface shape has reduced triangularity.

equilibrium. The surface is displaced downwards until it brushes against the limiter and used as the bounding surface in a fixed boundary equilibrium calculation.

The stability is determined using the PEST (Ref. 8) code. The mode of interest is the $n=1$ kink mode. Most of the studies set an ideal wall congruent with the vacuum vessel, free boundary calculations were also performed.

III. SURFACE CURRENT CALCULATION

A current flowing on a flux surface, ψ_s, has the general representation

$$\vec{j}_s = \vec{\nabla} \times (\kappa(\theta,\varphi)\vec{\nabla}\psi\delta(\psi-\psi_s)), \tag{1}$$

where κ is called the current potential and has units of amperes. The power that must be used to drive that current potential is

$$\frac{d\delta W}{dt} = -\int \vec{j}_s \cdot \vec{E} d^3x, \tag{2}$$

which can be rewritten using Faraday's law as

$$\frac{d\delta W}{dt} = \int \kappa \frac{\partial \vec{B}}{\partial t}\cdot\vec{\nabla}\psi\delta(\psi-\psi_s)\mathcal{J}d\psi d\theta d\varphi, \tag{3}$$

$$= \oint \kappa \frac{\partial \vec{B}}{\partial t}\cdot d\vec{a}. \tag{4}$$

The normal magnetic field can be expanded in orthonormal functions as

$$\vec{B}\cdot\hat{n} = w\sum_j \Phi_j(t) f_j(\theta,\varphi), \tag{5}$$

where $\oint w da = 1$ is a weight function and the expansion functions are defined so

$$\oint f_j f_k w da = \delta_{jk}. \tag{6}$$

The area element is $da = |\vec{\nabla}\psi|\mathcal{J}d\theta d\varphi$, where $\mathcal{J}$ is the coordinate Jacobian, and $d\vec{a} = \hat{n}da$.

The power equation, Eq. (3), can then be written as

$$\frac{d\delta W}{dt} = \sum_j \frac{d\Phi_j}{dt}\oint \kappa f_j w da. \tag{7}$$

If the current potential is expanded in terms of the same orthonormal functions, $\kappa = \sum_j I_j(t) f_j(\theta,\varphi)$, the energy equation becomes

$$\frac{d\delta W}{dt} = \sum_j \frac{d\Phi_j}{dt} I_j, \tag{8}$$

$$= \sum_{jk} \frac{d\Phi_j}{dt}\rho_{jk}\Phi_k, \tag{9}$$

where the linearity of the problem was used to write $I_j = \sum_k \rho_{jk}\Phi_k$.

The energy required to reach a certain point on a path defined by specified $\Phi_j(t)$ is $\delta W = \sum_{jk} \Phi_j \rho_{jk} \Phi_k / 2$. This result depends on the path taken through the space of the $\Phi_j(t)$ unless the matrix ρ_{jk} is symmetric as a differentiation, $d\delta W/dt$, of this expression for δW demonstrates. In ideal MHD, the energy is path independent, so ρ_{jk} is symmetric, which means the left and right eigenvectors of ρ_{jk} are identical. In other words, for a specific eigenvector of δW the same eigenfunction $f(\theta, \varphi)$ gives the flux and the current potential, and Eq. (3) implies the energy associated with the eigenfunction is $\delta W = I\Phi/2$.

The energy for a specific ideal MHD mode has the form $\delta W = I\Phi/2$, so the current I is trivially calculated once Φ is know. Since $\vec{B} \cdot \hat{n} = w\Phi f$ and $\oint f^2 w da = 1$,

$$\Phi^2 = \oint \frac{(\vec{B} \cdot \hat{n})^2}{w} da. \tag{10}$$

The normal component of the perturbed field, $\vec{Q} = \nabla \times \xi \times \vec{B}$, is given by,

$$\frac{\vec{Q} \cdot \nabla \psi}{|\nabla \psi|} = \frac{1}{R \mathcal{J} \nabla \psi |} \left(\frac{\partial \xi}{\partial \theta} + \frac{\partial \xi}{\partial \Phi} \right). \tag{11}$$

Here, R is the major radius, and $\mathcal{J}$ is the Jacobian. These are obtained from the post-processor of the PEST code.[10]

A. Normalization in the cylindrical limit

This approach, use of a linear model, requires additional information about the normalization. This is resolved by comparing with the cylindrical analytic model, described in Ref. 9.

Specifically, we approximate the straight system, with a circular cross-section tokamak with a large, but finite aspect-ratio, set equal to 20. The QSOLVER code,[7] where the safety-factor and pressure profile, and plasma geometry are prescribed, was used to obtain numerical equilibria. A negligible finite pressure was used, $\beta_N \sim 0.1$. The safety-factor profile is prescribed as

$$\mu(r) = \frac{4\mu_a}{1 + j_1} \left[\frac{1}{2} - (1 - j_1) \frac{r^2}{4a^2} \right] \tag{12}$$

with $\mu = 1/q$, μ_a defines the edge safety-factor and j_1 prescribes the shear.

Stability analysis and surface current evaluation were done using the procedure, described above. The surface current, J_s, computed here is the same as $\hat{i}^{surf}$, Eq. (20) of Ref. 9. Note that this is a dimensionless form and relates to the ratio of the surface current to the plasma current and that of the displacement, ξ, relative to the plasma radius, a

$$\mu_0 \frac{I_s}{I_p} = \hat{i}^{surf} \frac{\xi}{a}. \tag{13}$$

The results shown in Fig. 5 compare favorably with the results shown in Figure 2 of Ref. 9. Minor differences are attributable to the use of $f(\Psi)$ rather than $f(r)$, and the use of finite aspect ratio to represent the cylindrical limit.

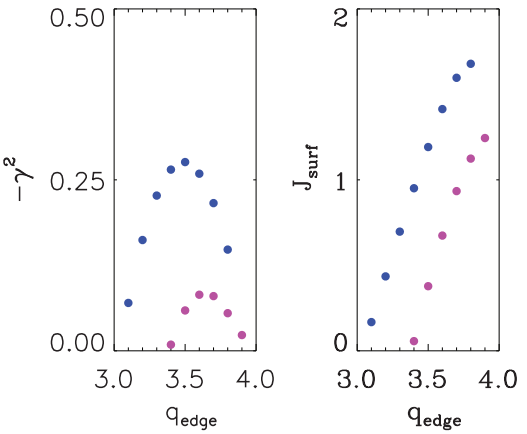

FIG. 5. Growth-rate of the free boundary $n = 1$, kink mode for the "cylindrical" model equilibria defined in Ref. 9, left panel. The blue dots correspond to $j_1 = 0.5$ and the magenta dots are for $j_1 = 0.25$b. The corresponding values of j_{surf}, Eq. (20) of Ref. 9, right panel.

IV. RESULTS

A. NSTX results

Shot 139540: An NSTX discharge, 139540, which ended in a disruption at $t \sim 0.34$ s, was analyzed. Figure 3 shows some of the salient observations. The figure shows the measured plasma current, I_p, which remains roughly constant, until $t = 0.334$ s, and then drops to zero in 2 ms. This drop is preceded by a rise in the measured halo currents. The halo currents are identified as a combination of an axisymmetric, $n = 0$, and non-axisymmetric, $n = 1$ components. Note that the figure shows the halo current density, the total current is estimated by integrating over the monitors. These currents reach values comparable to the plasma current

$$0.2 \leq \frac{I^{exp}_{halo}}{I_{plasma}} \leq 0.4. \tag{14}$$

The normalized pressure, β_N and estimates of q_{edge} are also shown. Note that q_{edge} decreases continuously, crossing $q = 3$ at about 330 ms, and $q = 2$ at 332 ms, approximately coincidental with a significant rise in the halo current. Figure 3 also shows the soft x-Ray, SXR, signal, which drops once at about 0.331 s, and collapses at about t = 0.3325 s, when the halo current rises sharply, an indicator of the thermal quench due to the instability.

We model the disruption using the equilibrium corresponding to 331 ms as the starting point. The modeling followed the procedure described in the section on plasma modeling. The results are shown in Fig. 6. A growing mode is first observed when q_{edge} drops below 3, rising sharply when q_{edge} drops below 2. The surface current required for equilibrium also rises rapidly at this point. It should be noted that while q_{edge} is reasonably well determined, the details of the profile in the core are not as precise. The figure also shows growth-rates and current fractions with no-wall boundary conditions and with the wall congruent to the vacuum vessel. Since the plasma is shrunken and shifted, see right panel of Fig. 4, the wall is close to the plasma in a limited region and far away for the rest of the surface, consequently its effect is negligible, for this case.

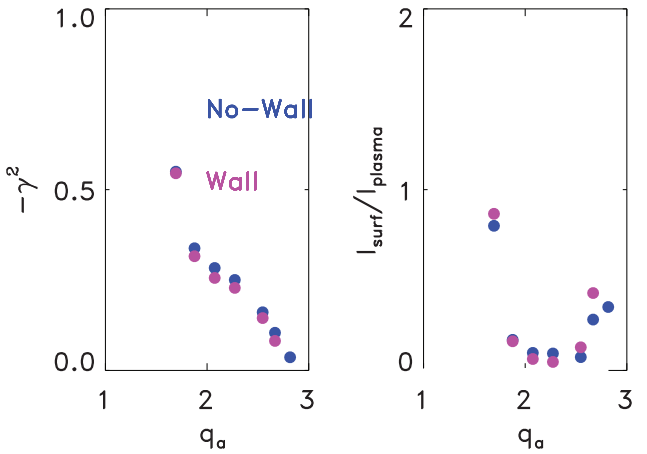

FIG. 6. Growth-rate of the free boundary kink mode for the simulated equilibria of NSTX discharge 139540, left, and surface curret required for equilibrium, right. Note that the I_{surf} required to maintain equilibrium is modest until q_{edge} drops below 2.

Shot 141641: This discharge had a slow VDE lasting about 15 ms. As the plasma drifts downwards, a small halo current is initially observed at $t = 0.527$ s, Fig. 7, which lasts for about 10 ms, followed by a sharp rise at $t = 0.537$ s, concurrently the current quench rate accelerates. It is also unusual, as q_{edge} is above 6 at the start of the VDE, and the final disruption occurs when $q_{edge} \approx 3$. Using the same procedure, described earlier, theoretical modeling shows that the kink mode is destabilized at high-q_{edge} and the surface currents mimic the behavior of the measured halo currents, Figure 8. Note that the SXR data were not available for this shot; however, the neutronics signal is shown. Its drop coincides with the first observation of halo currents.

We have compiled data from 33 discharges, which ended in disruptions. The modeling of q_{edge}, just before disruption, indicates that the majority of these discharges disrupted as q_{edge} dropped below 2, see Fig. 9.

The analysis of NSTX VDEs also indicates that when the kink mode's growth-rate is small, surface currents can provide stability, and disruptions occur only when $\gamma T_A \sim 0.5$, and $\frac{I_{surf}}{I_{plasma}} \sim 0.5$. Here, T_A refers to the Alfvénic time, characteristic of ideal MHD instabilities. This is an empirical model which fits the data from NSTX.

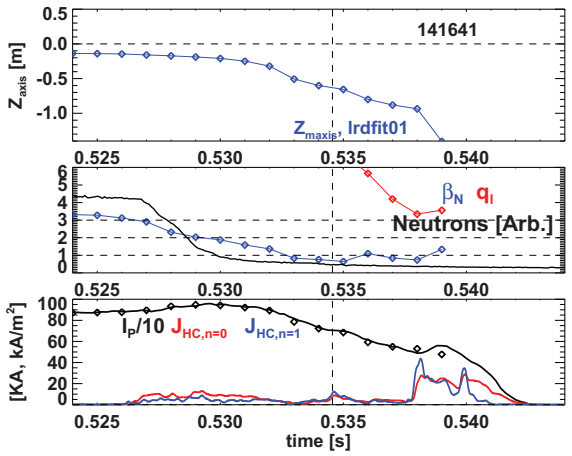

FIG. 7. Evolution of Z_{axis}, q_{edge}, and β_N, during the last 15 ms of a VDE in NSTX, shot No. 141641. (top two panels) The bottom panel shows the plasma current, black, and halo current measurements for $n = 0$, red; and $n = 1$, blue. Note that q_{edge} is continuously decreasing and drops to approximately 3.5 at $t = 0.538$ s. The halo current is first observed at about $t = 0.527$ s, when $q_{edge} \sim 8$.

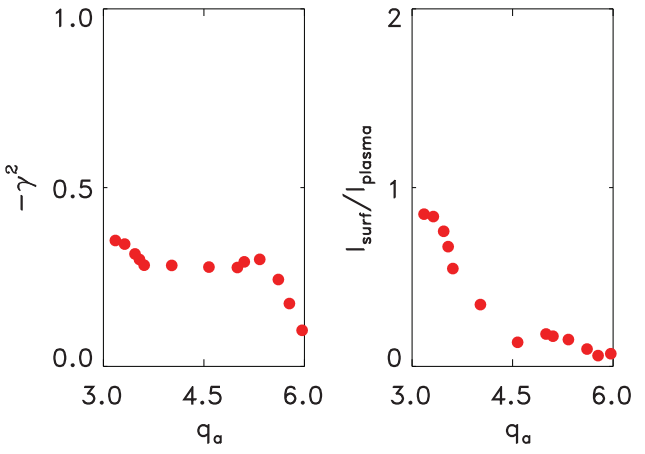

FIG. 8. Growth-rate of the free boundary kink mode for the simulated equilibria of NSTX discharge 141641, left, and surface current on the right. Note that this shot appears to survive for several milli-seconds after the onset of the kink, suggesting that the observed halo currents may be providing stability until q_{edge} approaches 3.

B. ITER geometry

We applied the same techniques to predict the likely behavior of an ITER discharge. We used a simple low-β L-mode equilibrium, and generated a sequence of shrinking equilibria. The results are shown in Figure 10. Here too, we find that the equilibrium sequence is stable until q_{edge} drops below three, when a marginally unstable mode is observed at $q_{\text{edge}} \sim 2.5$. However, as q drops below two, the growth-rate increases dramatically approaching unity, on the Alfven time scale. The surface current needed to maintain equilibrium is also shown in Fig. 10.

C. JET geometry

Simulation of the linear stability of the $n = 1$ kink mode in JET geometry shows similar results to the ITER case, i.e., a rapid growth of the instability for q less than 2. However, the mode is unstable for q larger than two. The surface

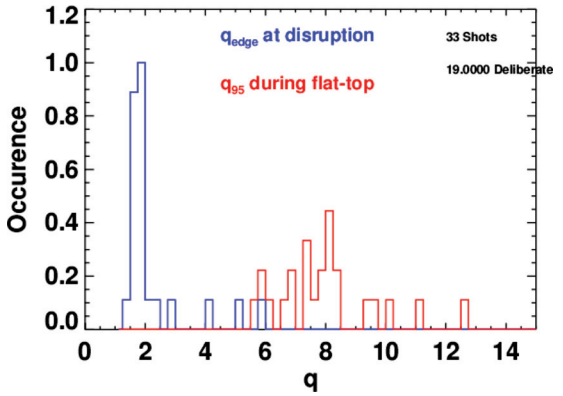

FIG. 9. Frequency of fast disruptions in deliberately induced VDEs. The edge safety-factor at the onset of the VDE, flat-top, and at the final disruption are shown in *red* and *blue*, respectively. Note that $q_{\text{edge}} = 2$ is the most likely value at disruption.

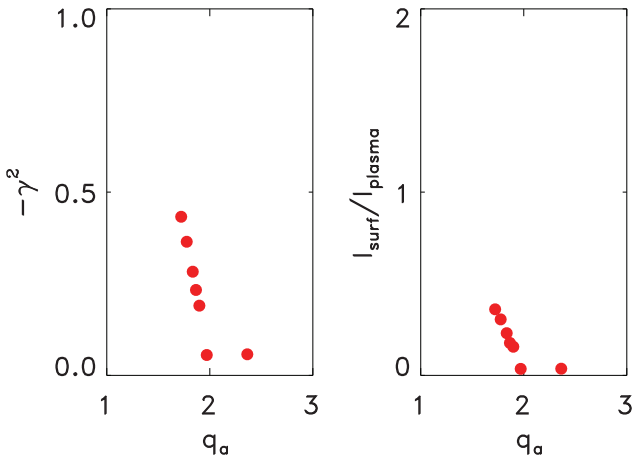

FIG. 10. (a) Growth-rate of the free boundary $n=1$, kink mode for ITER model equilibria. (b) The surface current required to maintain equilibrium.

current required for stability is approximately half the equilibrium plasma current, when q_{edge} drops below 2, Figure 11.

V. DISCUSSION

This report describes a practical approach to identifying the kink mode responsible for disruptions terminating some VDEs. Specifically it indicates that the $m/n=2/1$ kink mode, destabilized when $q_{edge}<2$ is the most likely signature of the onset of a disruption.

The role of the $n=0$ mode is more difficult to resolve. The mode is destabilized by ellipticity and is almost always unstable, the reason for a feedback system. We have estimated the surface current, using the same approach, and determined that the surface currents are of the same magnitude as the $n=1$ kink result. However, we note that our code does not include, the so called Lust-Martensen terms,[14] only relevant for $n=0$, and we did not include those results.

A method for determining the surface currents needed to maintain equilibrium was presented. Applications were made to model VDEs in NSTX. There is good correlation of the q_{edge} and stability between experiment and theory. In addition, the calculated surface currents were observed to reach the same magnitude as measured halo currents, suggesting that the two are related.

Although this study predicts Alfvénic growth-times, the expectation is that a halo current will arise to maintain force balance and the actual evolution takes place on the dissipative time scale of that current. Nevertheless, the mode's growth-rate is a measure of the strength of the instability, and the prescribed stability condition for the disruption is that the growth-rate is approximately half the Alfven time and the halo current is half the core plasma current. This empirical model describes the conditions, based on linear ideal MHD theory for the onset of disruption. However, the actual process is very likely more complex and requires additional physics.

This study focused on VDE related disruptions. However, the underlying theory should apply to all instabilities related to surface kinks, such as, high-beta kinks, Resistive Wall Modes (RWMs), and low-n Edge Localized Modes (ELMs). Evidence of such surface currents associated with ELMs was presented in Ref. 12, where the term SOLC, Scrape Off Layer Currents, was introduced. The theory presented here suggests that the SOLC may be the kink-driven surface currents. Another significant feature of this theory is that destabilization of the kink mode does not necessarily lead to an immediate termination of the discharge. Surface currents can provide a delayed response, if so, it raises the possibility of detecting SOL currents as a disruption precursor. We have examined the data base and observed that nearly all NSTX disruptions have some precursor, such as degradation of the confinement, increased flux consumption and large-scale MHD activity. Additionally, we often see a large spike in the halo current monitors a few milliseconds before the disruption, before there is any large vertical motion of the plasma. Further studies are required to determine if the SOL currents can be used as reliable disruption precursors.

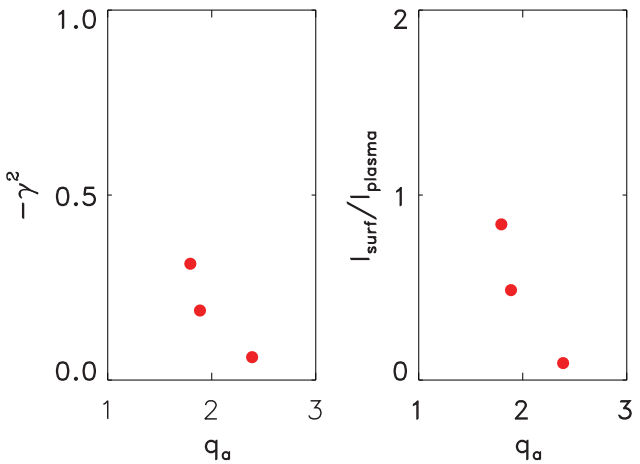

FIG. 11. (a) Growth-rate of the free boundary $n=1$, kink mode for model equilibria representing a VDE in JET geometry. (b) The surface current corresponding to the $n=1$ kink.

ACKNOWLEDGMENTS

This study benefited from Dr. L. Zakharov's insights on understanding and modeling disruptions in tokamaks. This manuscript has been authored by Princeton University and collaborators under Contract Number(s) DEAC0209CH11466 with the U.S. Department of Energy. The publisher, by accepting the article for publication, acknowledges that the United States Government retains a nonexclusive, paidup, irrevocable, worldwide license to publish or reproduce the published form of this manuscript, allow others to do so, for United States Government purposes.

[1]ITER Physics Basis, Nucl. Fusion **39**, 2137 (1999).
[2]L. Zakharov, Phys. Plasmas **15**, 062507 (2008).
[3]R. Fitzpatrick, Phys. Plasmas **16**, 012506 (2009).
[4]A. J. Webster, Phys. Plasmas **17**, 110708 (2010).
[5]H. R. Strauss, R. Paccagnella, and J. Breslau, Phys. Plasmas **17**, 082505 (2010).
[6]J. Menard, http://nstx-u.pppl.gov/software/lrdfit.
[7]J. Delucia, S. C. Jardin, and A. M. M. Todd, J. Comput. Phys. **37**, 183–204 (1980).
[8]R. C. Grimm, J. M. Greene, and J. L. Johnson, Methods Comput. Phys. **16**, 253 (1976).

[9]L. Zakharov, Phys. Plasmas **18**, 062503 (2011).
[10]S. Preische, J. Manickam, and J. L. Johnson, Comput. Phys. Commun. **76**, 318–325 (1993).
[11]S. P. Gerhardt, E. Fredrickson, L. Guttadora, R. Kaita, H. Kugel, J. Menard, and H. Takahashi, Rev. Sci. Instrum **82**, 103502 (2011).
[12]H. Takahashi, E. D. Fredrickson, and M. J. Schaeffer, Phys. Rev. Lett. **100**, 205001 (2008).
[13]S. P. Gerhardt, J. Menard, S. Sabbagh, and E. Scotti, Nucl. Fusion **52**, 063005 (2012).
[14]R. Lust and E. Martensen, Z. Naturforsch. A **13**, 706 (1960).